

Shifting Spotlight for Co-supervision: A Simple yet Efficient Single-branch Network to See Through Camouflage

Yang Hu¹, Jinxia Zhang^{*1,3}, Kaihua Zhang², Yin Yuan¹, Jiale Huang¹, Zechao Zhan¹, Xin Wang⁴

¹Key Laboratory of Measurement and Control of CSE, School of Automation, Southeast University, China

²School of Computer Science, Nanjing University of Information Science and Technology, China

³Advanced Ocean Institute of Southeast University, China ⁴Alibaba Group, China

Abstract—Camouflaged object detection (COD) remains a challenging task in computer vision. Existing methods often resort to additional branches for edge supervision, incurring substantial computational costs. To address this, we propose the Co-Supervised Spotlight Shifting Network (CS³Net), a compact single-branch framework inspired by how shifting light source exposes camouflage. Our spotlight shifting strategy replaces multi-branch designs by generating supervisory signals that highlight boundary cues. Within CS³Net, a Projection Aware Attention (PAA) module is devised to strengthen feature extraction, while the Extended Neighbor Connection Decoder (ENCD) enhances final predictions. Extensive experiments on public datasets demonstrate that CS³Net not only achieves superior performance, but also reduces Multiply-Accumulate operations (MACs) by 32.13% compared to state-of-the-art COD methods, striking an optimal balance between efficiency and effectiveness.

Index Terms—Camouflaged Object Detection, Network Co-supervision, Efficient Network Design.

I. INTRODUCTION

Camouflage is an evolutionary adaptation that allows animals to evade predators' attention by blending into the surroundings. This natural phenomenon has intrigued scientists and inspired diverse practical applications, such as detecting medical lesions [1]–[8] and identifying industrial defects [9]–[11]. Camouflaged Object Detection (COD) is particularly difficult because of the visually deceptive nature of camouflage. It often relies on the use of computationally intensive networks for accurate detection. Therefore, developing an efficient and effective COD method is of significant importance.

The major challenge of precisely segmenting camouflaged targets lies in the blurred boundaries between them and the surroundings. Recent deep learning based methods [12]–[16] effectively tackle this challenge by introducing an additional branch to integrate extra prior information (such as edge, depth, *etc.*). However, the additional branch substantially increases the number of parameters and computational demand, ultimately reducing the overall efficiency.

Corresponding author*. This work was supported by Research Fund for Advanced Ocean Institute of Southeast University, Nantong (GP202411), Guangdong Basic and Applied Basic Research Foundation (2022A1515011435), ZhiShan Scholar Program of Southeast University and the Fundamental Research Funds for the Central Universities, the Natural Science Basic Research Program of Shaanxi (Program No.2024JC-YBMS-513), and Key Research and Development Program of Zhejiang Province under Grants 2024C01025.

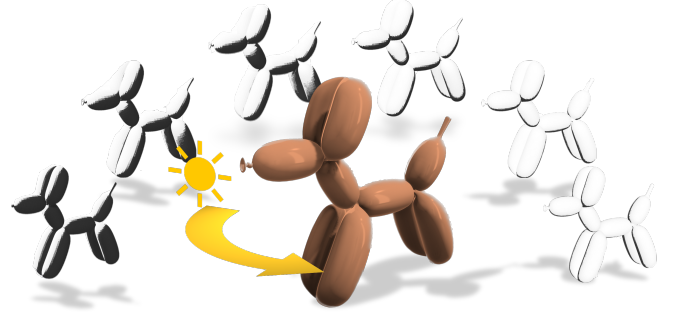


Fig. 1. An illustration of spotlight shifting strategy, the shadow projection over the balloon dog changes dramatically as the spotlight shifts from left to right. These changes highlight the object's contours, making them more distinct and easier to detect.

To address the inefficiencies caused by multi-branch structures, we propose a spotlight shifting strategy that enables network co-supervision within a single-branch framework. This strategy is inspired by how varying light condition can make the objects' contours more distinct. As presented in Fig. 1, the shifting light source leads to eye-catching changes on shadow projection, enhancing the visibility of the object. Our proposed spotlight shifting strategy mimics this effect by generating shadow maps with different spotlight positions, which are further used for co-supervision. This strategy allows the model to capture informative cues without extra branches.

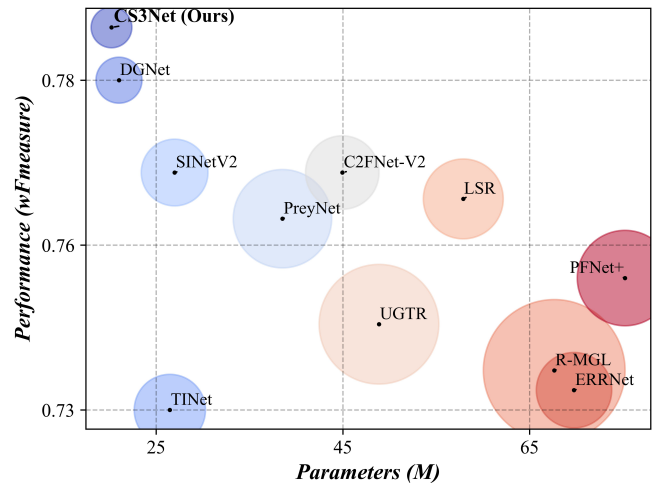


Fig. 2. Comparison of model performance (F_{β}^w on NC4K), parameters and MACs across state-of-the-art COD methods.

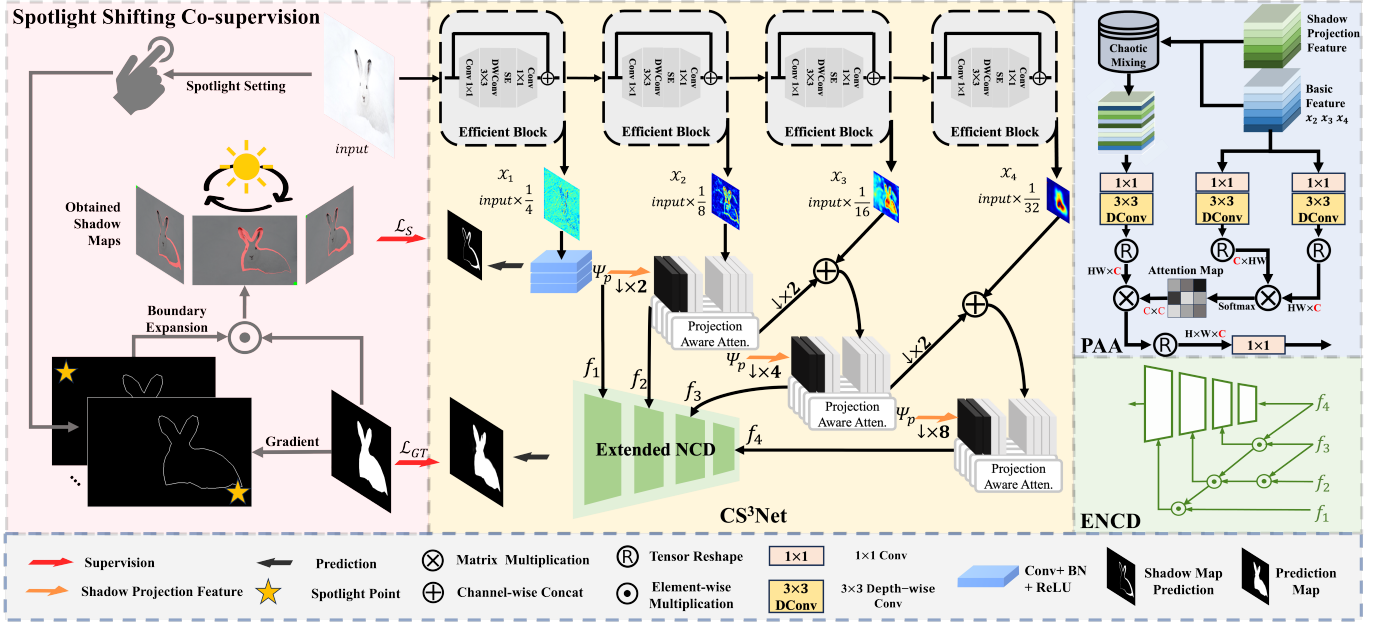


Fig. 3. The architecture of the proposed CS³Net. CS³Net operates as a single-branch network utilizing spotlight shifting strategy for co-supervision, it consists of two key modules: the Projection Aware Attention (PAA) and the Extended Neighbor Connection Decoder (ENCD) to integrate knowledge gained from co-supervision.

Our main goal is to develop a COD method that strikes the optimal performance-efficiency trade-off, as evidenced by Fig. 2. Targeting at which, we present the Co-Supervised Spotlight Shifting Network (CS³Net), a single-branch network that leverages spotlight shifting co-supervision for enhanced feature extraction. It integrates the proposed Projection Aware Attention (PAA) and Extended Neighbor Connection Decoder (ENCD) for feature refinement and precise prediction. Our contributions are summarized as follows:

- We propose spotlight shifting strategy for network co-supervision that enriches the model capability to discern camouflaged objects without introducing extra branches, providing a unique perspective in COD domain.
- Based on spotlight shifting strategy, a novel single-branch and efficient model, termed as CS³Net is crafted for COD task. It integrates the proposed PAA, and ENCD to precisely enhance feature representations.
- CS³Net achieves the optimal balance between model efficiency and performance, reducing MACs by 32.13% compared to the most advanced efficient COD models, while also delivering superior performance.

II. THE PROPOSED METHOD

As illustrated in Fig. 3, CS³Net is a single-branch network that leverages Spotlight Shifting Co-supervision to refine feature extraction. The network first employs EfficientNet [17] to capture multi-scale features $\{x_i\}_{i=0}^4$, followed by the Projection Aware Attention (PAA) to progressively align attention with shadow projection feature. Finally, the Extended Neighbor Connection Decoder (ENCD) efficiently fuses these refined features to improve prediction accuracy.

A. Spotlight Shifting Strategy

Motivation. To achieve effective co-supervision within a single-branch framework, a straightforward yet information-

dense prior must be devised. Drawing inspiration from the observation that shadow projection over an object undergoes eye-catching changes as the light source shifts its position, which makes blurred edge details easier to recognize. This concept serves as the basis for simulating the shadow projection effect in our algorithm.

Shadow Projection Effect Simulation. The shadow projection over an object is influenced by the position of the light source. To replicate this effect, we devise an algorithm that takes a ground truth map and selected points to produce shadow maps (\mathcal{M}_S), as illustrated in the left panel of Fig. 3. Typically, shadow projections over an object form near its boundary, so the edge map (\mathcal{M}_E) is first extracted by computing the gradient of the ground truth map (\mathcal{M}_{GT}). To generate the shadow map based on a specific spotlight point q with coordinates (q_x, q_y) , every point $p_i \in \mathcal{M}_E$ with coordinates $(p_{i,x}, p_{i,y})$ undergoes circular dilation $\delta_{d_i}(\cdot)$, the dilation radius d_i is determined by the Euclidean distance between p_i and q . $\delta_{d_i}(\cdot)$ overlays a circle centered at p_i with the radius d_i , scaled to a range of 0 to 30 before dilation. This function outputs a binary dilation map where the dilated area around p_i is marked as 1, and elsewhere as 0:

$$\begin{aligned} d_i(p_i, q) &= \sqrt{(p_{i,x} - q_x)^2 + (p_{i,y} - q_y)^2} \quad \forall p_i \in \mathcal{M}_E, \\ \Delta(p_i) &= \delta_{d_i(p_i, q)}(p_i) \quad \forall p_i \in \mathcal{M}_E. \end{aligned} \quad (1)$$

To ensure that the desired shadow map \mathcal{M}_S is within the ground truth map \mathcal{M}_{GT} , the following function is applied:

$$\mathcal{M}_S = \mathcal{M}_{GT} \odot \left(\bigcup_{p_i \in \mathcal{M}_E} \Delta(p_i) \right), \quad (2)$$

where \odot denotes element-wise multiplication, and \cup represents the union of all dilation results.

TABLE I

QUANTITATIVE COMPARISON ON THREE DATASETS, WITH THE BEST SCORES HIGHLIGHTED IN **BOLD**. METHODS INVOLVING EFFICIENT DESIGN ARE SELECTIVELY HIGHLIGHTED FOR COMPARISON.

Models	Pub./Year	Params. (M) ↓	MACs (G) ↓	NC4K [18]				CAMO [19]				COD10K [20]			
				$S_\alpha \uparrow$	$E_\phi \uparrow$	$F_\beta^w \uparrow$	$MAE \downarrow$	$S_\alpha \uparrow$	$E_\phi \uparrow$	$F_\beta^w \uparrow$	$MAE \downarrow$	$S_\alpha \uparrow$	$E_\phi \uparrow$	$F_\beta^w \uparrow$	$MAE \downarrow$
SINet [20]	CVPR ₂₀	48.95	19.42	0.808	0.871	0.723	0.058	0.745	0.804	0.644	0.092	0.776	0.864	0.631	0.043
UGTR [21]	ICCV ₂₁	48.87	127.12	0.839	0.874	0.747	0.052	0.785	0.823	0.686	0.086	0.818	0.853	0.667	0.035
R-MGL [14]	CVPR ₂₁	67.64	249.89	0.833	0.867	0.740	0.052	0.775	0.812	0.673	0.088	0.814	0.852	0.666	0.035
LSR [18]	CVPR ₂₁	57.90	25.21	0.840	0.865	0.766	0.048	0.787	0.838	0.696	0.080	0.804	0.880	0.673	0.037
TINet [22]	AAAI ₂₁	26.47	15.96	0.829	0.879	0.734	0.055	0.781	0.836	0.678	0.087	0.793	0.861	0.635	0.042
C2FNet-V2 [23]	TCSVT ₂₂	44.94	18.10	0.840	0.896	0.770	0.048	0.799	0.859	0.730	0.077	0.811	0.887	0.691	0.036
PreyNet [24]	MM ₂₂	38.53	58.10	0.834	0.899	0.763	0.050	0.790	0.842	0.708	0.077	0.813	0.881	0.697	0.034
SINet-V2 [25]	TPAMI ₂₂	26.98	12.28	0.847	0.903	0.770	0.048	0.820	0.882	0.743	0.070	0.815	0.887	0.680	0.037
diffCOD [26]	ECAI ₂₃	—	—	0.837	0.891	0.761	0.051	0.795	0.852	0.704	0.082	0.812	0.892	0.684	0.036
PFNet+ [27]	SCIS ₂₃	75.22	51.41	0.831	0.889	0.754	0.052	0.791	0.850	0.713	0.080	0.806	0.880	0.677	0.037
WS-SAM [28]	NIPS ₂₄	—	—	0.829	0.886	0.802	0.052	0.759	0.818	0.742	0.092	0.803	0.878	0.719	0.038
Efficiency Considered Methods															
ERRNet [13]	PR ₂₂	69.76	20.05	0.827	0.887	0.737	0.054	0.779	0.842	0.679	0.077	0.786	0.867	0.630	0.043
DGNet [29]	MIR ₂₃	21.02	2.77	0.857	0.911	0.784	0.042	0.839	0.901	0.769	0.057	0.822	0.896	0.693	0.033
CS ³ Net (Ours)	—	20.52	1.88	0.859	0.915	0.792	0.042	0.839	0.903	0.774	0.057	0.825	0.901	0.703	0.032

Shadow Projection Feature Extraction. Unlike other co-supervised networks [12]–[16] with dual-branch architectures, we only use 4 layers of convolution to extract the shadow projection feature Ψ_p and predict the shadow map \mathcal{P}_s , minimizing computational demand and parameters:

$$\Psi_p = Bconv_{k=3}^{iter=3}(x_1), \quad \mathcal{P}_s = Bconv_{k=1}^{iter=1}(\Psi_p). \quad (3)$$

Here, $Bconv_k^{iter}(\cdot)$ involves a $k \times k$ convolution, batch normalization, and ReLU, repeated $iter$ times.

B. Projection Aware Attention

The PAA module leverages the shadow projection feature Ψ_p and the concatenated output of the preceding PAA with $\{x_i\}_{i=2}^4$ to generate refined features $\{f_i\}_{i=1}^4$. This process uses “chaotic mixing” ($Mix(\cdot, \cdot)$), which randomly concatenates and shuffles input channels. Following [30], the PAA captures global and local contexts using 3×3 depth-wise ($DConv(\cdot)$) and point-wise ($PConv(\cdot)$) convolutions:

$$\begin{aligned} f_1 &= \Psi_p, \\ f_i^c &= \mathcal{D}^2(f_{i-1}) \oplus x_i, \\ \mathcal{K}_i &= \mathcal{V}_i = DConv(PConv(f_i^c)), \\ \mathcal{Q}_i &= DConv(PConv(Mix(\mathcal{D}^{2^{i-1}}(\Psi_p), f_i^c))), \\ f_i &= PConv\left(\text{softmax}\left(\frac{\mathcal{Q}_i \mathcal{K}_i^T}{\alpha}\right) \mathcal{V}_i\right), \text{ for } i = 2, 3, 4, \end{aligned} \quad (4)$$

where $\mathcal{D}^n(\cdot)$ is n -fold down-sampling, \oplus indicates channel concatenation, and α is a learnable scaling factor.

C. Extended Neighbor Connection Decoder

Building on the idea of neighbor connection [25], we extend an extra path for high-resolution feature, which is normally discarded yet crucial for detail reconstruction. The ENCD combines multi-scale features $\{f_i\}_{i=1}^4$ while maintaining semantic consistency. These features are transited to N_C channels via point-wise convolution before ENCD. As shown in the bottom right of Fig. 3, the feature aggregation strategy can be expressed as:

$$\begin{cases} f'_4 = f_4, \\ f'_3 = f_3 \odot \mu^2(Bconv_3(f_4)), \\ f'_2 = f_2 \odot \mu^2(Bconv_3(f_3)) \odot \mu^2(Bconv_3(f'_3)), \\ f'_1 = f_1 \odot \mu^2(Bconv_3(f'_2)), \end{cases} \quad (5)$$

where f_i and f'_i denote the features before and after the neighbor connection. $\mu^2(\cdot)$ and \odot represent two times up-sampling and element-wise multiplication respectively. Using the refined features $\{f'_i\}_{i=1}^4$, the decoding process is:

$$\begin{aligned} \mathcal{P}_{GT} &= Bconv_1(\mathcal{F}(\mathcal{F}(\mathcal{F}(f'_4, f'_3), f'_2), f'_1)), \\ \text{where } \mathcal{F}(x, y) &= Bconv_3(Bconv_3(\mu^2(x)) \oplus y). \end{aligned} \quad (6)$$

In this context, \mathcal{P}_{GT} represents the final prediction, and \oplus denotes channel-wise concatenation.

D. Loss Function and Co-supervision

As the algorithm described in Sec. II-A, different shadow maps are synthesized into a unified one via pixel-wise addition. This map serves as a critical supervisory element, informing the calculation of the shadow map loss \mathcal{L}_S by assessing the mean squared error (MSE) between \mathcal{P}_S and \mathcal{M}_S .

The total loss \mathcal{L} is a combination of \mathcal{L}_S and the ground truth loss \mathcal{L}_{GT} . The latter consists of the weighted Intersection over Union (IoU), L_{IoU}^w , and weighted binary cross-entropy (BCE), L_{BCE}^w , as used in the literature [20], [25], [29], [31]. The complete loss function can be expressed as:

$$\mathcal{L} = \mathcal{L}_{GT}(\mathcal{P}_{GT}, \mathcal{M}_{GT}) + \mathcal{L}_S(\mathcal{P}_S, \mathcal{M}_S). \quad (7)$$

III. EXPERIMENTS AND RESULTS

A. Experiment Settings

Datasets. In line with most COD methods, our model is trained on the COD10K [20] and CAMO [19] datasets, and tested on the NC4K [18], COD10K, and CAMO datasets. CAMO contains 1,250 images, with 1,000 used for training and 250 for testing. COD10K consists of 5,066 images, with 3,040 for training and 2,026 for testing. NC4K is a challenging test dataset comprising 4,121 images.

Metrics. Following previous works [14], [18], [21], [25], four widely used metrics are employed for evaluation: Mean Absolute Error (MAE), Mean E-measure (E_ϕ) [32], S-measure (S_α) [33], and Weighted F-measure (F_β^w) [34]. To assess the efficiency of our method¹, the number of model parameters (in

¹The model efficiency is ascertained using the flops-counter toolbox: <https://github.com/sovrasov/flops-counter.pytorch>

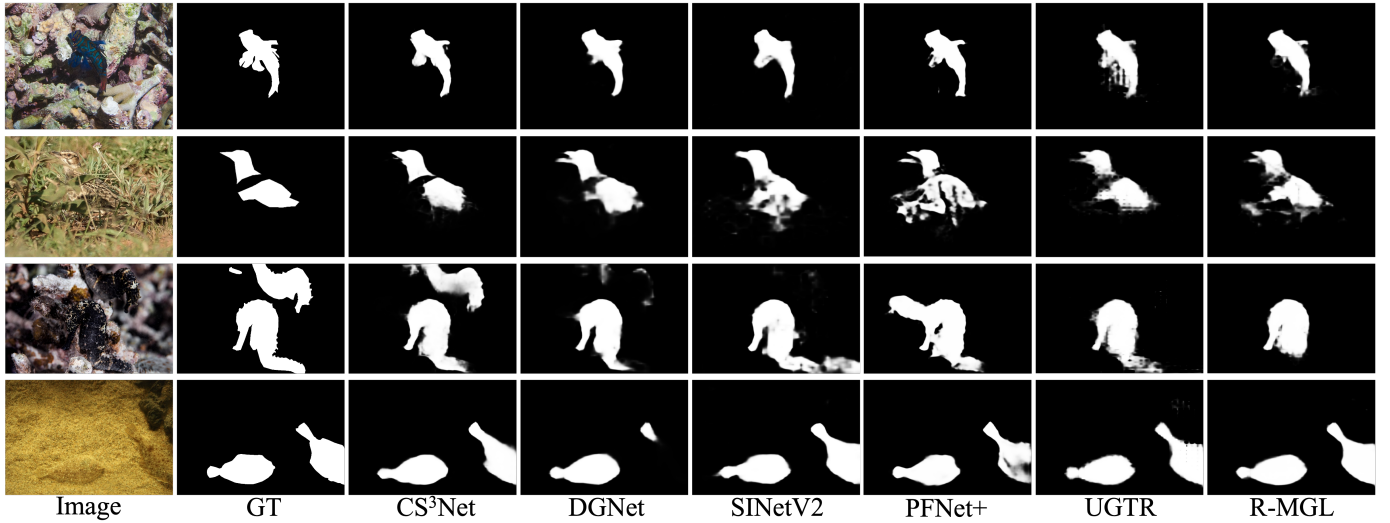


Fig. 4. Visual performance of CS³Net and other highly competitive COD methods.

Millions, M) and the quantity of multiply-accumulate (MACs) operations (in Giga, G) are used as indicators.

Implementation Details. Our model is trained on a single NVIDIA RTX-3090 GPU. The training settings including optimizer, image resizing and data augmentation mirror those found in [29]. The PAA is configured with 4 heads (N_H) and the N_C of ENCD is set to 32. The shadow map is generated using the spotlight shifting strategy, with the top-left and bottom-right of the image preset as spotlight points.

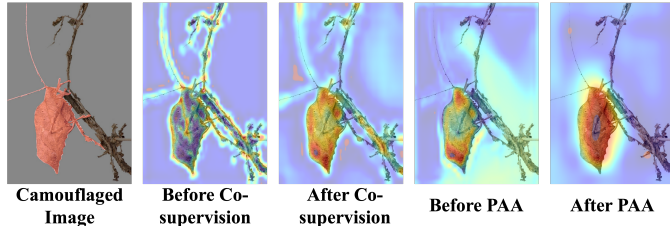


Fig. 5. Visualization of feature maps before and after proposed modules: Spotlight Shifting Co-supervision and PAA.

B. Comparison with the State-of-the-Art Methods

Our CS³Net is benchmarked against recent SOTA methods, including 2 efficiency focused methods. For fair competition, all results are derived either directly from the associated publications or by reproducing with the default configurations. As presented in Tab. I, our model demonstrates exceptional performance across all datasets with a notable reduction in MACs (32.13% drop compared to the leading efficiency focused method, DGNet [29]) and smaller model size. Specifically, CS³Net achieves higher S_α score than SINet-V2 [25] by 2.86% in NC4K and improves F_β^w score by 3.38% in COD10K. Fig. 4 clearly demonstrates the superiority of our model in accurately segmenting multiple camouflaged objects and those partially occluded by surrounding elements.

C. Ablation Study

Tab. II presents our ablation study, where we also compare the effects of different co-supervision strategies on our method. Here, the term “baseline” refers to the EfficientNet-B4 with

TABLE II
ABLATION STUDY ON THE CAMO DATASET.

Method	CAMO			
	$S_\alpha \uparrow$	$E_\phi \uparrow$	$F_\beta^w \uparrow$	$MAE \downarrow$
Baseline	0.798	0.804	0.643	0.084
Baseline+ENCD	0.829	0.889	0.761	0.061
Baseline+ENCD+PAA (w/o Co-supervision)	0.832	0.890	0.752	0.062
Our Method Edge Map	0.835	0.898	0.768	0.059
Dilated Edge	0.835	0.897	0.760	0.061
Spotlight Shifting	0.839	0.903	0.774	0.057

convolution layers to replace other modules.

Effectiveness of ENCD. Tab. II demonstrates that the ENCD module is crucial for enhancing the model’s performance, as evidenced by the significant improvement in all metrics.

Effectiveness of PAA. PAA alone shows limited improvement as it relies on the integration of informative cues from co-supervision. However, when combined with co-supervision, it significantly boosts performance (last 3 rows of Tab. II), Fig. 5 further shows that the feature map highlights the camouflaged objects more distinctly when PAA is applied.

Effectiveness of Spotlight Shifting. Tab. II demonstrates that the spotlight shifting strategy provides superior performance compared to using edge or dilated edge co-supervision. Specifically, spotlight shifting achieves the best results across all key metrics. And it effectively suppresses irrelevant features and highlights the essential regions, as shown in Fig. 5.

IV. CONCLUSION

Our research introduces a novel single-branch efficient network, CS³Net for camouflaged object detection. The model leverages the spotlight shifting strategy to simulate the shadow projection effect, enhancing the visibility of camouflaged objects. And we proposes PAA for feature aggregation and ENCD for efficient decoding. Extensive experiments show that CS³Net strikes the optimal balance between performance and efficiency, achieving a 32.13% reduction in MACs compared to the cutting-edge efficient COD methods, while enhancing detection accuracy, indicating a step forward in performance-conscious COD model design.

REFERENCES

- [1] D.-P. Fan, G.-P. Ji, T. Zhou, G. Chen, H. Fu, J. Shen, and L. Shao, "Pranet: Parallel reverse attention network for polyp segmentation," in *MICCAI*. Springer, 2020, pp. 263–273.
- [2] C.-C. Chiao, J. K. Wickiser, J. J. Allen, B. Genter, and R. T. Hanlon, "Hyperspectral imaging of cuttlefish camouflage indicates good color match in the eyes of fish predators," *Proceedings of the National Academy of Sciences*, vol. 108, no. 22, pp. 9148–9153, 2011.
- [3] G.-P. Ji, Y.-C. Chou, D.-P. Fan, G. Chen, H. Fu, D. Jha, and L. Shao, "Progressively normalized self-attention network for video polyp segmentation," in *MICCAI*. Springer, 2021, pp. 142–152.
- [4] G.-P. Ji, G. Xiao, Y.-C. Chou, D.-P. Fan, K. Zhao, G. Chen, and L. Van Gool, "Video polyp segmentation: A deep learning perspective," *Machine Intelligence Research*, vol. 19, no. 6, pp. 531–549, 2022.
- [5] D.-P. Fan, T. Zhou, G.-P. Ji, Y. Zhou, G. Chen, H. Fu, J. Shen, and L. Shao, "Inf-net: Automatic covid-19 lung infection segmentation from ct images," *IEEE TMI*, vol. 39, no. 8, pp. 2626–2637, 2020.
- [6] Y.-H. Wu, S.-H. Gao, J. Mei, J. Xu, D.-P. Fan, R.-G. Zhang, and M.-M. Cheng, "Jcs: An explainable covid-19 diagnosis system by joint classification and segmentation," *IEEE TIP*, vol. 30, pp. 3113–3126, 2021.
- [7] J. Liu, B. Dong, S. Wang, H. Cui, D.-P. Fan, J. Ma, and G. Chen, "Covid-19 lung infection segmentation with a novel two-stage cross-domain transfer learning framework," *Medical Image Analysis*, vol. 74, p. 102205, 2021.
- [8] W.-C. Chen, X.-Y. Yu, and L.-L. Ou, "Pedestrian attribute recognition in video surveillance scenarios based on view-attribute attention localization," *Machine Intelligence Research*, vol. 19, no. 2, pp. 153–168, 2022.
- [9] P. Bergmann, S. Löwe, M. Fauser, D. Sattlegger, and C. Steger, "Improving unsupervised defect segmentation by applying structural similarity to autoencoders," *arXiv preprint arXiv:1807.02011*, 2018.
- [10] D. Tabernik, S. Šela, J. Skvarč, and D. Skočaj, "Segmentation-based deep-learning approach for surface-defect detection," *Journal of Intelligent Manufacturing*, vol. 31, no. 3, pp. 759–776, 2020.
- [11] D.-M. Tsai, S.-K. S. Fan, and Y.-H. Chou, "Auto-annotated deep segmentation for surface defect detection," *IEEE Transactions on Instrumentation and Measurement*, vol. 70, pp. 1–10, 2021.
- [12] Z. Wu, L. Su, and Q. Huang, "Stacked cross refinement network for edge-aware salient object detection," in *ICCV*, October 2019.
- [13] G.-P. Ji, L. Zhu, M. Zhuge, and K. Fu, "Fast camouflaged object detection via edge-based reversible re-calibration network," *PR*, vol. 123, p. 108414, 2022.
- [14] Q. Zhai, X. Li, F. Yang, C. Chen, H. Cheng, and D.-P. Fan, "Mutual graph learning for camouflaged object detection," in *CVPR*, 2021, pp. 12 997–13 007.
- [15] C. He, K. Li, Y. Zhang, L. Tang, Y. Zhang, Z. Guo, and X. Li, "Camouflaged object detection with feature decomposition and edge reconstruction," in *CVPR*, 2023, pp. 22 046–22 055.
- [16] D. Sun, S. Jiang, and L. Qi, "Edge-aware mirror network for camouflaged object detection," in *ICME*. IEEE, 2023, pp. 2465–2470.
- [17] M. Tan and Q. Le, "Efficientnet: Rethinking model scaling for convolutional neural networks," in *ICML*. PMLR, 2019, pp. 6105–6114.
- [18] Y. Lv, J. Zhang, Y. Dai, A. Li, B. Liu, N. Barnes, and D.-P. Fan, "Simultaneously localize, segment and rank the camouflaged objects," in *CVPR*, 2021, pp. 11 591–11 601.
- [19] T.-N. Le, T. V. Nguyen, Z. Nie, M.-T. Tran, and A. Sugimoto, "Anabran network for camouflaged object segmentation," *Computer Vision and Image Understanding*, vol. 184, pp. 45–56, 2019.
- [20] D.-P. Fan, G.-P. Ji, G. Sun, M.-M. Cheng, J. Shen, and L. Shao, "Camouflaged object detection," in *CVPR*, 2020.
- [21] F. Yang, Q. Zhai, X. Li, R. Huang, A. Luo, H. Cheng, and D.-P. Fan, "Uncertainty-guided transformer reasoning for camouflaged object detection," in *ICCV*, 2021, pp. 4146–4155.
- [22] J. Zhu, X. Zhang, S. Zhang, and J. Liu, "Inferring camouflaged objects by texture-aware interactive guidance network," in *AAAI*, vol. 35, no. 4, 2021, pp. 3599–3607.
- [23] G. Chen, S.-J. Liu, Y.-J. Sun, G.-P. Ji, Y.-F. Wu, and T. Zhou, "Camouflaged object detection via context-aware cross-level fusion," *IEEE TCSVT*, vol. 32, no. 10, pp. 6981–6993, 2022.
- [24] M. Zhang, S. Xu, Y. Piao, D. Shi, S. Lin, and H. Lu, "Preynet: Preying on camouflaged objects," in *ACM MM*, 2022, pp. 5323–5332.
- [25] D.-P. Fan, G.-P. Ji, M.-M. Cheng, and L. Shao, "Concealed object detection," *IEEE transactions on pattern analysis and machine intelligence*, vol. 44, no. 10, pp. 6024–6042, 2021.
- [26] Z. Chen, R. Gao, T.-Z. Xiang, and F. Lin, "Diffusion model for camouflaged object detection," *arXiv preprint arXiv:2308.00303*, 2023.
- [27] H. Mei, X. Yang, Y. Zhou, G. Ji, X. Wei, and D. Fan, "Distraction-aware camouflaged object segmentation," *SCIEN-TIA SINICA Informationis (SSI)*, vol. 3, p. 7, 2023.
- [28] C. He, K. Li, Y. Zhang, G. Xu, L. Tang, Y. Zhang, Z. Guo, and X. Li, "Weakly-supervised concealed object segmentation with sam-based pseudo labeling and multi-scale feature grouping," *NIPS*, vol. 36, 2024.
- [29] G.-P. Ji, D.-P. Fan, Y.-C. Chou, D. Dai, A. Liniger, and L. Van Gool, "Deep gradient learning for efficient camouflaged object detection," *Machine Intelligence Research*, vol. 20, pp. 92–108, 2023.
- [30] S. W. Zamir, A. Arora, S. Khan, M. Hayat, F. S. Khan, and M.-H. Yang, "Restormer: Efficient transformer for high-resolution image restoration," in *CVPR*, 2022, pp. 5728–5739.
- [31] J. Wei, S. Wang, and Q. Huang, "F³net: fusion, feedback and focus for salient object detection," in *AAAI*, vol. 34, no. 07, 2020, pp. 12 321–12 328.
- [32] D.-P. Fan, G.-P. Ji, X. Qin, and M.-M. Cheng, "Cognitive vision inspired object segmentation metric and loss function," *Scientia Sinica Informationis*, vol. 6, no. 6, 2021.
- [33] D.-P. Fan, M.-M. Cheng, Y. Liu, T. Li, and A. Borji, "Structure-measure: A new way to evaluate foreground maps," in *ICCV*, 2017, pp. 4548–4557.
- [34] R. Margolin, L. Zelnik-Manor, and A. Tal, "How to evaluate foreground maps?" in *CVPR*, 2014, pp. 248–255.